PHYSICS OF FLUIDS **26**, 072104 (2014)

# Post-breakup solutions of Navier-Stokes and Stokes threads

J. Eggers
*School of Mathematics, University of Bristol, University Walk, Bristol BS8 1TW, United Kingdom*

(Received 26 September 2013; accepted 2 July 2014; published online 21 July 2014)

We consider the breakup of a fluid thread, neglecting the effect of the outside fluid (or air). After breakup, the solution of the fluid equations consists of two threads, receding rapidly from the point of breakup. We show that the bulk of each thread is described by a similarity solution of slender geometry (which we call the thread solution), but which breaks down near the tip. Near the tip of the thread the thread solution can be matched to a solution of Stokes' equation, which consists of a finger of constant spatial radius, rounded at the end. Very close to breakup, the thread solution balances inertia, viscosity, and surface tension (Navier-Stokes case). If however the fluid viscosity is large (as measured by the dimensionless Ohnesorge number), some time after breakup the thread solution consists of a balance of surface tension and viscosity only (Stokes case), and the thread profile can be described analytically.  [http://dx.doi.org/10.1063/1.4890203]

## I. INTRODUCTION

The breakup of a piece of fluid into two is a generic occurrence in free surface flow, and is relevant to the description of sprays, in printing, and for many other applications.[1,2] At the point of breakup the continuum description breaks down, so it is not clear how to continue the solution across the singularity, for example, when integrating the equations of fluid motion numerically. Here we address this issue, by constructing a solution valid after breakup, which is the unique continuation of the similarity solution describing the pinching of a Newtonian fluid thread asymptotically close to breakup.[2,3] This similarity solution, representing a balance of surface tension, inertia, and viscosity, has been confirmed both by experiment[4,5] and numerical simulations.[6] However, when the thread radius falls below a certain viscosity-dependent scale, the thread becomes sensitive to thermal noise, leading to a more complicated structure of nested similarity solutions.[7] Here we will only deal with the deterministic equations, and will not address the issues of noise. We also neglect the effect of any outer fluid, such as air.[8]

The problem of continuation has been resolved fully for the breakup of an axisymmetric, purely inviscid fluid neck, in which case the pre-breakup similarity solution is controlled by a single length scale.[2,9,10] The same similarity description applies to the post-breakup solution, which was treated in Ref. 11. Solutions of a similar type (namely, the recoil of an inviscid fluid wedge) had already been considered in Ref. 12, using the method of similarity solutions. To solve the similarity equations, one still needs to solve an irrotational flow problem with a free surface, but the time dependence has been eliminated. If further assumptions on the slenderness of the initial fluid wedge are made, the complexity of the problem reduces further, and analytical solutions are available, see, e.g., Ref. 13.

However, asymptotically close to breakup the assumption of inviscid flow always breaks down and viscosity becomes important, even if it is small.[2] For this reason, and to describe fluids with larger viscosity, we need to consider viscous similarity solutions (Navier-Stokes and Stokes problems), for which the radial length scale becomes asymptotically small compared to the axial scale,[2] and the profile is slender. We aim to find a post-breakup solution, which consists of two disconnected pieces of fluid, each of which corresponds to a liquid thread receding rapidly from the point of breakup. The technical problem that is encountered is that while the bulk of the thread is described

 

by a similarity solution (of the same structure as the solution before breakup), the slenderness assumption underlying the solution breaks down at the tip, where the profile must be rounded.

Difficulties of this type are encountered frequently in lubrication or long-wavelength problems, for example, at the end of a drop,[14] the rim of a liquid sheet,[15] or at corners.[16] A geometry similar to that of receding thread also occurs in the case of two bubbles, coalescing in a viscous medium.[17] In Ref. 14, it was argued that in some cases, such as a drop hanging from a faucet, the end is effectively in static equilibrium. Hence, it can be treated by supplementing the long-wavelength equations with the full expression for the mean curvature. In Ref. 18, conditions introduced at the end point lead to an unphysical finite-time singularity at the tip, after which the model description breaks down. Another solution is needed near the end, to be matched to the long-wavelength model.

The continuation of the pre-breakup solution to times after rupture was first treated in Ref. 19 for the Navier-Stokes case. It was shown that each receding thread is again described by a similarity solution, which satisfies the requirement that it has to match the pre-breakup solution away from the pinch point. Since the geometry is slender, the problem is reduced to a set of ordinary differential equations.[3] However, an additional boundary condition is still missing at the tip, which in Ref. 19 was derived from a regularity condition, imposed on phenomenological grounds. This leads to a unique solution of the similarity problem after breakup.

An alternative procedure has been used to treat the Navier-Stokes and Stokes problems,[20] based on the idea of a liquid quasi-spherical "blob" at the end of the thread, that picks up mass as the jet retracts. Originally, this approach had been applied to inviscid problems.[21–24] The "blob" solution at the end is chosen so as to satisfy global mass and momentum conservation; however, this does not determine the shape of the blob. In fact, we know that in the case of the inviscid post-breakup solution,[11] the end is part of the similarity solution, and not in quasistatic equilibrium. The spherical shape used in Ref. 20 also does not match the similarity solution in the viscous thread; in addition, the initial condition for the similarity solution will depend on the point where the two solutions are patched together.

In the present paper we address the matching problem between the viscous, slender similarity solution describing the bulk of the receding thread and the tip region, see Fig. 1. The overall shape of the thread is shown in the inset. We show that at the tip we need to solve the full axisymmetric flow problem. In a local frame of reference, the inertial contributions drop out, so one only has to solve

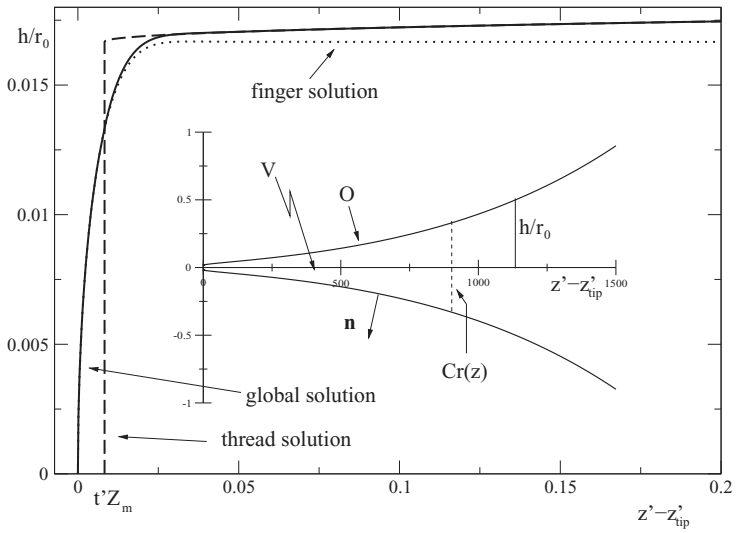


FIG. 1. Inset: the receding thread as constructed in this paper for Stokes flow at a dimensionless time $t' = 0.1$ after breakup. Lengths are measured with respect to some externally prescribed scale $r_0$. Main figure: a blowup of the radius function $h(z, t)$ near the tip. The dashed line is the self-similar solution to the long-wavelength equations (the thread solution), valid away from the tip; its end is shifted by $t'Z_m$ relative to the tip position $z'_{tip}$. The dotted line is a solution to the axisymmetric Stokes equation (the finger solution), valid near the tip. They can be combined to construct a global solution (solid line).

Stokes' equation. As noticed in Ref. 15 for the case of a receding viscously dominated sheet, the fluid swept up by the end leads to a spatially uniform increase in thickness, and does not collect into a blob at the end of the thread. Thus the "inner solution" (in the language of matched asymptotics[25]) consists of a finger receding at constant speed, and whose spatial scale increases linearly in time, as well as uniformly in space (Fig. 1, dotted line). We will call this inner solution the "finger solution."

The finger solution matches the similarity solution describing the receding liquid thread away from the tip (Fig. 1, dashed line); this is known as the "outer solution" in matched asymptotics. We will call this part of the solution the "thread solution." The matching condition for the receding thread results in the same tip condition already used in Ref. 19 for the construction of the similarity solution, but in a more rigorous fashion. In addition, we now supply the correct solution on the scale of the tip. The solid line is the global solution to the receding thread problem, obtained by combining inner and outer solutions into a composite solution,[25] as we will describe later on.

This paper is organized as follows: We begin with the case of a very viscous fluid, which means that the dimensionless Ohnesorge number,[2]

$$Oh = \frac{\eta}{\sqrt{\rho r_0 \gamma}}, \tag{1}$$

is very large. Here $\eta$ is the fluid viscosity, $\rho$ is the density, $\gamma$ the surface tension, and $r_0$ is a length scale prescribed externally. Then excluding a short time after breakup, inertia can be neglected everywhere, not just at the tip. As a result, the thread solution (outer solution) can be obtained analytically, which simplifies the treatment.

Next we construct the finger (or inner) solution from Stokes' equation with a free surface, and show that it matches the outer thread solution. We then show that the same matching can be achieved for the similarity solution with inertia (the Navier-Stokes case), which is generic in the sense that it is always seen asymptotically close to breakup. Finally, we discuss possible experimental verification of the observed scaling.

## II. SELF-SIMILAR STOKES SOLUTION

To construct the similarity solution valid away from the tip, we first derive the long-wavelength equations valid for a slender thread, which become particularly simple if inertia is neglected.[2] The main complication in finding the pre-breakup solution lies in the appearance of a non-local constraint,[26,27] which corresponds to the tensile force $T(t)$ inside the fluid thread, see Ref. 28. In Subsection II A we show, starting from the Stokes equation, that this force is zero after the thread has broken, which is clear on physical grounds. This greatly simplifies the problem, and permits to find a similarity solution in analytical form.

### A. Slender thread description

Consider an axisymmetric piece of fluid which ends in a tip (see the inset of Fig. 1), at the apex of which the local radius $h(z, t)$ goes to zero. Without inertia, the interior of the thread is described by Stokes' equation, subject to a normal stress $\gamma\kappa\mathbf{n}$, where $\mathbf{n}$ is the outward normal to the surface; $\kappa$ is (twice) the mean curvature of the interface, given by

$$\kappa = \frac{1}{h(1+\partial_z h^2)^{1/2}} - \frac{\partial_{zz} h}{(1+\partial_z h^2)^{3/2}} \tag{2}$$

for an axisymmetric surface. The expression (2) remains finite as the tip is approached. If $\boldsymbol{\sigma}$ is the stress tensor, the equations can be summarized concisely by

$$\nabla \cdot \boldsymbol{\sigma} = 0 \quad \text{in the thread}, \qquad \boldsymbol{\sigma} \cdot \mathbf{n} = -\gamma \mathbf{n}\kappa \quad \text{on the surface}. \tag{3}$$

We follow the arguments of Ref. 29 to show that the tensile force vanishes in the configuration shown in Fig. 1. Integrating $\nabla \cdot \boldsymbol{\sigma}$ over a volume $V$ bounded by the thread surface and a plane perpendicular to the axis, we find from the divergence theorem and from the boundary condition

that

$$0 = \int_S \mathbf{n}\cdot\boldsymbol{\sigma} dS = \int_{Cr(z)} \mathbf{n}\cdot\boldsymbol{\sigma} dS + \int_O \mathbf{n}\cdot\boldsymbol{\sigma} dS = \int_{Cr(z)} \mathbf{e}_z\cdot\boldsymbol{\sigma} dS - \gamma\int_O \mathbf{n}\kappa dS, \tag{4}$$

where $Cr(z)$ is the cross section of the thread at $z$, and $O$ is the open surface from $Cr(z)$ to the end of the thread.

It follows from the surface divergence theorem (see Ref. 30, p. 239) that

$$\int_O \mathbf{n}\kappa dS = -\int_{\partial O} \mathbf{m} ds, \tag{5}$$

where

$$\mathbf{m} = \frac{\mathbf{e}_r\partial_z h + \mathbf{e}_z}{(1+\partial_z h^2)^{1/2}} \tag{6}$$

is tangential to the surface $O$, and pointing away from $V$. Performing the line integral along the circumference of $O$ on the right-hand side of (5), the radial component of (6) drops out, and we obtain

$$\int_O \mathbf{n}\kappa dS = -\frac{2\pi h\mathbf{e}_z}{(1+\partial_z h^2)^{1/2}}. \tag{7}$$

Combining (4) and (7), we arrive at the exact relation[29]

$$\int_0^{h(z,t)} \mathbf{e}_z\cdot\boldsymbol{\sigma} r dr = -\frac{\gamma\mathbf{e}_z h}{(1+\partial_z h^2)^{1/2}} \tag{8}$$

for the force balance on the cross section of the thread. Multiplying (8) by the basis vector $\mathbf{e}_z$, this gives

$$\int_0^{h(z,t)} \left(-p + 2\eta\frac{\partial v_z}{\partial z}\right) r dr = -\frac{\gamma h}{(1+\partial_z h^2)^{1/2}}, \tag{9}$$

where $p(r, z, t)$ is the pressure, and $v_z(r, z, t)$ is the axial component of the velocity.

In a region where the thread is slender we have, following Ref. 31, p. 887,

$$p(r, z, t) = \gamma/h - \eta\partial_z v_0 + O(r^2, r\partial_z h, \partial_z h^2), \tag{10}$$

where $v_z(z, r, t) = v_0(z, t) + O(r^2)$. Thus performing the integral over the radius in (8) we have

$$\frac{h^2}{2}\left(\frac{\gamma}{h} - 3\eta\partial_z v_0\right) = \gamma h,$$

where we have used that $\partial_z h \ll 1$. In other words,

$$0 = \gamma h + 3\eta\partial_z v_0 h^2, \tag{11}$$

which is the standard result for a slender thread,[2] but with vanishing tensile force $T(t) = 0$ on the left-hand side. The equation of motion for $h(z, t)$ is the statement of mass conservation:[2]

$$\frac{\partial h}{\partial t} + \partial_z\left(v_0 h^2\right) = 0. \tag{12}$$

To simplify (11) further, we pass from an Eulerian to a Lagrangian description, where $z(s, t)$ is the position of a fluid volume, labeled by $s$.[2] With the transformations

$$\frac{\partial z}{\partial s} = \frac{1}{h^2}, \quad \frac{\partial z}{\partial t} = v_0, \tag{13}$$

mass conservation (12) is satisfied identically. Introducing the Lagrangian profile $h(z, t) = H(s, t)$, (11) transforms into[2]

$$\frac{\partial H}{\partial t} = \frac{v_\eta}{6}, \tag{14}$$

where $v_\eta = \gamma/\eta$ is the capillary speed. Equation (14) is the desired slender thread description in Lagrangian variables.

### B. Thread solution

We begin with what will be the outer solution in our matching problem, describing the receding thread, except for a small region near the tip. It is shown as the dashed line in Fig. 1. We write the solution to (14) in the form of a similarity solution:

$$H = t' r_0 \chi_a(\zeta), \quad \zeta = s'/t'^{\delta}, \tag{15}$$

where $\chi_a(\zeta)$ is the similarity function in Lagrangian coordinates; $t' = v_\eta(t - t_0)/r_0$ is the dimensionless time distance from breakup, and $s' = (s - s_0)/r_0^3$ the corresponding spatial variable. Here $r_0$ is a length scale prescribed externally, chosen the same as before breakup; $s_0$ and $t_0$ are the particle label and the time, respectively, where breakup occurs. The two pieces of the post-breakup solution are the mirror images of one another. Therefore, we will consider only the case $\zeta > 0$. The main difference from the pre-breakup solution is that $t'$ is chosen with the opposite sign, making it positive for $t > t_0$. The axial similarity exponent $\delta$ is as yet undetermined. Using (15), (14) transforms

$$\chi_a - \delta\zeta\chi_a' = 1/6, \tag{16}$$

where the prime denotes the derivative with respect to the argument. The similarity equation (16) has the solution

$$\chi_a = \chi_- \zeta^{1/\delta} + 1/6, \tag{17}$$

with $\chi_-$ a constant of integration.

To find $\chi_-$ and $\delta$, we demand that (17) matches the pre-breakup solution:[19] in the limit $t' \to 0$, both solutions have to coincide at some finite spatial distance $\Delta$ away from the pinch point. This means that the similarity solution $\chi_a$ after breakup must have the same asymptotic behavior for $\zeta \to \infty$ as the similarity solution $\chi_b$ before breakup, found in Ref. 26. It was shown in Ref. 27 that the only *stable* pre-breakup solution has the axial exponent $\delta_0 \approx 2.175$, while the asymptotic behavior is $\chi_b \approx \chi_m \zeta^{1/\delta_0}$, where $\chi_m = 1/(12(\delta_0 - 1))$. For this to match to (17) for $\zeta \to \infty$, we identify $\chi_- = \chi_m$ and $\delta = \delta_0$, which determines all the free parameters of the post-breakup solution. In summary, the profile of the post-breakup solution is

$$\chi_a = \chi_m \zeta^{1/\delta} + 1/6, \quad \delta = 2.1748717\ldots. \tag{18}$$

To calculate the velocity $v_m$ of the end of the thread, we note that using (13),

$$\frac{\partial v_0}{\partial s} = \frac{\partial (H^{-2})}{\partial t} = -\frac{2}{H^3}\frac{\partial H}{\partial t} = -\frac{v_\eta}{3H^3}. \tag{19}$$

The end is located at $\zeta = 0$ in similarity variables, since it must be at a constant value $s = 0$ in Lagrangian coordinates. We will see below that the end of the thread solution does not exactly correspond to the tip of the whole solution, since there is a small part of the finger solution that protrudes from it, see Fig. 1. Integrating from a point in the bulk to the end, we find in the limit $t' \to 0$:

$$\frac{v_m}{v_\eta} = \frac{1}{3}\int_0^\infty \frac{ds}{H^3} = \frac{t'^{\delta-3}}{3}\int_0^\infty \frac{d\zeta}{\chi_a^3} = A t'^{\delta-3}, \tag{20}$$

where

$$A = \frac{\pi 2^{2-\delta} 3^{3-\delta}\delta(1-\delta)(2-\delta)}{3\chi_m^\delta \sin(\pi\delta)} \approx 620.5\ .$$

To find the actual shape of the thread solution in real space, we have to integrate the first transformation of (13) over $s$. In Eulerian coordinates, the similarity form of the profile is[2]

$$h(z,t) = t' r_0 \phi_a(\xi), \quad \xi = \frac{z'}{t'^{\beta}}, \tag{21}$$

where $\beta = \delta - 2 \approx 0.175$, and $z' = (z - z_0)/r_0$, with $z_0$ the point of breakup. Thus from the first equation of (13), the transformation is

$$\frac{d\xi}{d\zeta} = \frac{1}{\phi_a^2} = \frac{1}{\chi_a^2}. \tag{22}$$

To find the similarity profile $\phi_a(\xi)$ after breakup, we integrate (22) using (18) to find

$$\xi - \xi_m = \int_0^{\left(\frac{\phi_a - 1/6}{\chi_m}\right)^\delta} \frac{d\zeta}{\left(1/6 + \chi_m \zeta^{1/\delta}\right)^2}. \tag{23}$$

Here $\xi_m$ is the end of the thread solution in similarity variables: $z'_m = \xi_m t'^\beta$, and thus

$$v_m = v_\eta \xi_m \beta t^{\beta - 1}. \tag{24}$$

Comparing this to (20), we obtain $\xi_m = A/\beta$.

We call the thread profile given by (21), (23) the (Stokes) thread solution, shown in Fig. 4 below. The integral in (23) can be written in terms of Lerch's $\Phi$ function,[32] but for the purposes of matching it is more useful to have an accurate description near the end. Expanding the integrand, we have

$$\left(1/6 + \chi_m \zeta^{1/\delta}\right)^{-2} = 36\left(1 - 12\chi_m \zeta^{1/\delta}\right) + O(\zeta^{2\delta}),$$

and thus

$$\Delta\xi \equiv \xi - \xi_m = 36\left[\left(\frac{\phi_a - 1/6}{\chi_m}\right)^\delta - \frac{12\chi_m}{1 + 1/\delta}\left(\frac{\phi_a - 1/6}{\chi_m}\right)^{1+\delta}\right].$$

Solving for $\phi_a$, we obtain

$$\phi_a = \frac{1}{6} + \chi_m \left(\frac{\Delta\xi}{36}\right)^{1/\delta}\left[1 + \frac{12\chi_m}{1+\delta}\left(\frac{\Delta\xi}{36}\right)^{1/\delta} + O\left(\Delta\xi^{2/\delta}\right)\right]. \tag{25}$$

To obtain an analytical expression for the thread *far* from the end, we found it useful to derive an alternative expression to (23). To this end we rewrite (22) in the form

$$\frac{d\xi}{d\phi_a}\frac{d\phi_a}{d\zeta} = \frac{1}{\phi_a^2},$$

and calculate $\dfrac{d\phi_a}{d\zeta}$ from (18) with $\phi_a = \chi_a$. The result is

$$\frac{d\xi}{d\phi_a} = \frac{\delta}{\chi_m^\delta}\frac{(\phi_a - 1/6)^{\delta-1}}{\phi_a^2}, \tag{26}$$

which can be integrated to yield[33]

$$\Delta\xi = \frac{\delta}{\chi_m^\delta}\int_{1/6}^{\phi_a}\frac{(\phi - 1/6)^{\delta-1}}{\phi^2}d\phi = \frac{\delta}{\chi_m^\delta}\left[\frac{\phi_a^{\delta-2}}{\delta - 2}F\left(2-\delta, 1-\delta; 3-\delta; \frac{1}{6\phi_a}\right) - \frac{\pi(\delta-1)6^{2-\delta}}{\sin(\pi\delta)}\right]. \tag{27}$$

Using the series expansion of the hypergeometric function $F$ to first order, this yields

$$\phi_a = \frac{1-\delta}{6(3-\delta)} + \left[(\delta-2)\frac{\chi_m^\delta}{\delta}\Delta\xi + \frac{\pi(\delta-2)(\delta-1)6^{2-\delta}}{\sin(\pi\delta)}\right]^{1/(\delta-2)} + O\left(\Delta\xi^{1/(2-\delta)}\right), \tag{28}$$

which turns out to be a good approximation to the full profile for $\phi_a \gtrsim 1/3$.

Similarly, to calculate the similarity function $\psi_a(\xi)$ of the Eulerian velocity field $v_0$, defined by

$$v_0(z, t) = v_\eta t'^{\beta-1}\psi_a(\xi), \tag{29}$$

we use (19) to obtain

$$\frac{\partial\psi_a}{\partial\xi} = -\frac{1}{3\phi_a}. \tag{30}$$

Combining this with (26) we have

$$\frac{d\psi_a}{d\phi_a} = -\frac{\delta}{3\chi_m^\delta}\frac{(\phi_a - 1/6)^{\delta-1}}{\phi_a^3}, \tag{31}$$

which is integrated to give

$$\psi_a - \psi_m = -\frac{\delta}{3\chi_m^\delta}\int_{1/6}^{\phi_a}\frac{(\phi - 1/6)^{\delta-1}}{\phi^3}d\phi = -\frac{\delta}{3\chi_m^\delta}\left[\frac{\phi_a^{\delta-3}}{\delta-3}F\left(3-\delta, 1-\delta; 4-\delta; \frac{1}{6\phi_a}\right)\right.$$
$$\left. + \frac{\pi(\delta-1)(\delta-2)6^{3-\delta}}{2\sin(\pi\delta)}\right], \tag{32}$$

where $\psi_m = \xi_m\beta$ according to (24). To obtain an expansion of $\psi_a$, valid near the end, we use (30) together with the expansion (25) to obtain

$$\psi_a = \psi_m - \Delta\xi\left[2 - \frac{12\chi_m\delta}{1+\delta}\left(\frac{\Delta\xi}{36}\right)^{1/\delta} + O\left(\Delta\xi^{2/\delta}\right)\right]. \tag{33}$$

## III. MATCHING

The most striking property of the similarity solution (25) is that $\phi_a = 1/6$ is finite at the end $\xi = \xi_m$, so that $h_m = r_0 t'/6 = v_\eta(t - t_0)/6$, whereas clearly the radius should be zero at the tip (see Fig. 1, dashed line). The reason is that near the tip the axial scale is comparable to the radial scale, which is different from the scaling of the thread solution (21). Demanding that the radial scales match, we have

$$\Delta_{tip}^{(ax)} \propto \Delta_{tip}^{(r)} \propto \Delta_{thread}^{(r)} \propto t', \quad \Delta_{thread}^{(ax)} \propto t'^{\beta}, \tag{34}$$

where $\Delta^{(r)}$ and $\Delta^{(ax)}$ refer to the radial and axial scales, respectively, of the finger solution and the thread solution, see Fig. 1. Since $\beta \approx 0.175 < 1$, $\Delta_{tip}^{(ax)} \ll \Delta_{thread}^{(ax)}$ in the limit $t' \to 0$, which means that on the scale of the thread solution, the tip is of vanishing size, corresponding to a jump from zero to 1/6 in similarity variables.

To explain why the matching between the finger and the thread solutions works, consider (25), valid near the tip. It follows that the slope of the interface for $\Delta\xi \lesssim 1$ is to leading order given by

$$\partial_z h = t'^{1-\beta}\phi_a'(\xi) = t'^{1-\beta}\frac{\chi_m}{36\delta}\left(\frac{\Delta\xi}{36}\right)^{-\frac{1+\beta}{2+\beta}}. \tag{35}$$

To show that this is consistent with a finger of constant width near the tip, we have to identify an overlap region whose typical scale is intermediate between $\Delta_{tip}^{(ax)}$ and $\Delta_{thread}^{(ax)}$ (Ref. 25, p. 57). We choose $\Delta_{match}^{(ax)} = t'^{3/4}$, which will also serve us in the Navier-Stokes case to be discussed below; any power between $\beta$ and 1 would have done. Evaluating the slope (35) at $\Delta_{match}^{(ax)}$, we find $\Delta\xi_{match} = t'^{3/4-\beta}$, and so $\partial_z h \propto t'^{\frac{5-3\beta}{8+4\beta}} \to 0$ in the matching region. Thus the receding thread in the matching region looks indeed like a finger, which we will describe now. Note that (35), evaluated in the limit $\Delta\xi \to 0$ at constant $t'$, in fact diverges. However, this would correspond to both inner and outer variables going to zero; what is relevant to the matching is the consistency of both inner and outer solutions in an intermediate region of overlap. We will demonstrate the matching using a more formal expansion of the inner and outer solutions in Subsection III B below.

### A. Finger solution

The inner solution (or finger solution) consists of a finger of constant spatial radius. As an illustration, we show the simulation of a retracting cylindrical drop, which is rounded at the end, in Fig. 2; inertial effects have been neglected. Similar simulations, but for the case of arbitrary viscosity, have been carried out in Refs. 34 and 35. Steady retraction was found for large viscosities, while a bulbous end forms as viscosity is decreased. An analogous solution in two dimensions

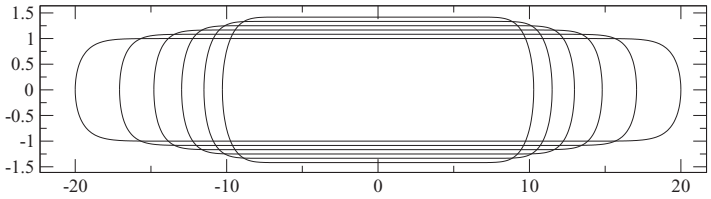


FIG. 2. A cylindrical viscous drop retracts under the action of surface tension, as described by Stokes' equation. As the drop shortens, it becomes thicker, but retains its cylindrical shape away from the tip. The receding tip is described by the thread solution (40), (41) below. The boundary integral method used to simulate the free-surface dynamics is that of Ref. 29.

(a retracting sheet) has been studied in Ref. 15, using long-wavelength theory. It was found that in the limit of large viscosities, the thickness of the sheet increased uniformly, without forming a "blob" at the end, just as seen in Fig. 2 for the axisymmetric case. Both the axial and radial scales expand linearly in time, and the shape of the finger converges onto a universal similarity profile, which we describe now. We begin with the solution far away from the tip, where the radius is uniform. Let us take the apex of the finger to be at the origin, with the cylindrical drop to the right. Far away from the tip, we expect the flow field to be a uniform extensional flow

$$v_z(z,r,t) = -az/t, \quad v_r(z,r,t) = ar/2t, \tag{36}$$

where $a$ is a constant and $v_z$ is determined up to an additive constant only. This is an exact solution of Stokes' equation at constant pressure, as we show now.

Integrating $\partial_t h(z,t) = v_r(z,h,t)$, we find that the finger radius is

$$h = h_0 t^{a/2}. \tag{37}$$

From the normal stress boundary condition, we find

$$p = \frac{\gamma}{h} + 2\eta \frac{\partial v_r}{\partial r},$$

which is indeed constant in space. Combining with (9) and integrating over the radius, we have that

$$\frac{h^2}{2}\left(-\frac{\gamma}{h} + 3\frac{\partial v_z}{\partial z}\right) = -\gamma h,$$

having used $\partial_z h = 0$. Inserting (36) and (37), it follows that

$$3\frac{a}{t} = -3\frac{\partial v_z}{\partial z} = \frac{v_\eta}{h} = \frac{v_\eta t^{-a/2}}{h_0},$$

and so $a = 2$ and $h_0 = v_\eta/6$. In conclusion, the finger width behaves like

$$h_f = \frac{v_\eta t}{6}, \tag{38}$$

matches (21), (25), while the velocity field away from the tip is

$$v_z(z,r,t) = -2z/t + const, \quad v_r(z,r,t) = r/t. \tag{39}$$

This suggests a similarity solution for the finger in which all length scales are rescaled by $t$. If $\mathbf{x}(q) = (z(q), r(q))$ is a parametric representation of the retracting finger (with its apex chosen as the origin), we are looking for similarity solutions

$$\mathbf{x} = v_\eta(t - t_0)\mathbf{X} \equiv t' r_0 \mathbf{X}, \tag{40}$$

where the prefactor $t' r_0$ corresponds to that of the thread solution (21). If, in addition, $\mathbf{v}(q) = (v_z(q), v_r(q))$ is the velocity on the surface, in view of (39) the velocity is in similarity form

$$\mathbf{v} = v_\eta \mathbf{V}. \tag{41}$$

In components, the similarity functions are $\mathbf{X}(Q) = (Z(Q), R(Q))$ and $\mathbf{V}(Q) = (V_z(Q), V_r(Q))$, where $Q$ parameterizes the similarity profile. According to (38), we have that far from the tip the

finger radius is $R = 1/6$ in similarity variables, while (39) becomes $V_z = -2Z + V_m$ and $V_r = R$, where $V_m$ is a constant to be determined.

The free surface condition for the motion of the interface reads

$$\left(\frac{\partial \mathbf{x}(q)}{\partial t} - \mathbf{v}(q)\right) \cdot \mathbf{n} = 0, \tag{42}$$

which in similarity variables becomes

$$(\mathbf{X}(Q) - \mathbf{V}(Q)) \cdot \mathbf{N} = 0, \tag{43}$$

where $\mathbf{N}$ is the normal to the similarity profile.

To find the velocity on the boundary, we use a boundary integral description. In the case of a drop of viscosity $\eta$ with an inviscid exterior, the equation reads[2]

$$\frac{\mathbf{v}(\mathbf{x}_1)}{2} = -v_\eta \int_S \kappa \mathbf{J}\mathbf{n}\, \mathrm{d}S_2 + \int_S \mathbf{v}\mathbf{K}\mathbf{n}\, \mathrm{d}S_2, \tag{44}$$

where $\mathbf{J}$ and $\mathbf{K}$ are the free-space Green's functions

$$\mathbf{J}(\mathbf{r}) = \frac{1}{8\pi}\left[\frac{\mathbf{I}}{r} + \frac{\mathbf{rr}}{r^3}\right], \quad \mathbf{K}(\mathbf{r}) = -\frac{3}{4\pi}\frac{\mathbf{rrr}}{r^5}, \quad \mathbf{r} = \mathbf{x}_1 - \mathbf{x}_2, \tag{45}$$

and $S$ is the surface of the drop. Using the similarity transformations (40) and (41), (44) becomes

$$\frac{\mathbf{V}(\mathbf{x}_1)}{2} = -\int_S \kappa_s \mathbf{J}\mathbf{N}\, \mathrm{d}S_2 + \int_S \mathbf{V}\mathbf{K}\mathbf{N}\, \mathrm{d}S_2, \tag{46}$$

where $\kappa_s$ is the mean curvature of the similarity profile. To determine the finger solution, we have to solve Eqs. (43) and (46), subject to the boundary conditions

$$V_r = R = 1/6, \quad V_z = -2Z + V_m, \tag{47}$$

for $Z \to \infty$, and $R = V_z = 0$ at the tip $Z = 0$.

To find the similarity solution numerically, we use a version of the code that produced Fig. 2. Every few time steps, all coordinates were rescaled so as to keep the drop radius at the asymptotic value of 1/6, in accordance with (47). This causes the drop to become shorter, so in the same step, an extra piece of fluid was inserted at the center of the drop, to keep the drop length at a value 20 times longer than its radius. This ensures that the two tips do not influence each other, and that far from the tip, the velocity field has its asymptotic form given by the boundary condition (47).

The similarity solution obtained from this computation is shown in Fig. 3. It is seen that the finger solution quickly reaches a constant radius of 1/6, and that the radial and axial components of the velocity field have the expected asymptotics (47), with $V_m \approx 0.25$. Inserting the similarity profiles into (43), we have confirmed that the kinematic condition is verified to less than 1% of the

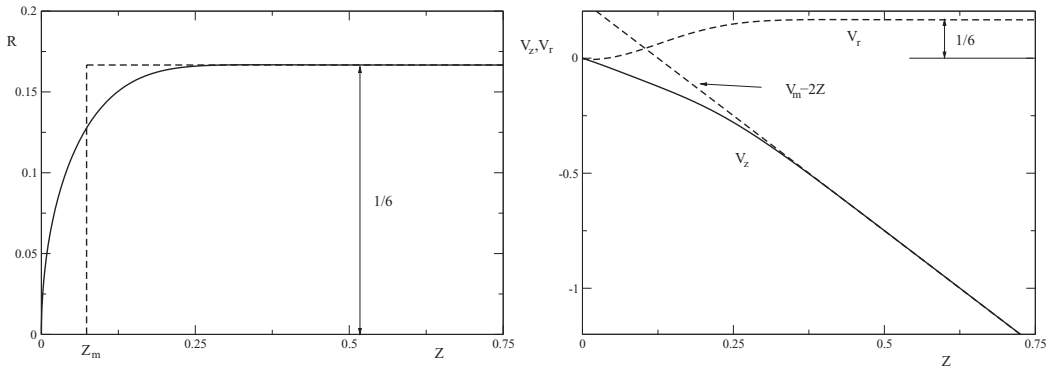


FIG. 3. Similarity solution of the retracting finger. The profile is shown on the left, where the dashed line indicates a cylinder of constant radius having the same volume. The radial and axial components of the velocity field at the surface are on the right, with the asymptotic behavior for large $Z$ indicated.

size of the individual terms. A similar similarity solution should exist in the large viscosity limit of a retracting sheet.[15] Note that while the flow field is fully three-dimensional at the tip in both problems, we found that a naive long-wavelength solution, based on (11) but with $1/h$ replaced by the mean curvature (2), yields a solution which is rather close to the true profile based on the full Stokes equation.

Indeed, to understand the *approach* of the profile $R(Z)$ toward its uniform value $R = 1/6$ as $Z \to \infty$ one can use the long-wavelength equations (11) and (12), since the solution is very close to being flat. We use a similarity ansatz analogous to (40), (41):

$$h = v_\eta(t - t_0)R(Z), \quad v_0 = v_\eta V(Z), \tag{48}$$

where $Z = z/(v_\eta(t - t_0))$. Inserting into (11), (12), we find

$$R - ZR' + R'VRV'/2 = 0, \quad 3V'R = -1, \tag{49}$$

where the prime denotes differentiation with respect to $Z$. Eliminating $V$ between the two equations, we arrive at

$$R''(1 - 6R) = \frac{2R'^2}{R}. \tag{50}$$

Writing $R(Z) = 1/6 + \epsilon(Z)$, we find

$$\epsilon''\epsilon = -2\epsilon'^2,$$

whose only decaying solution is $\epsilon = B/Z$, so that

$$R(Z) = \frac{1}{6} + \frac{B}{Z} + O(Z^{-2}) \tag{51}$$

for $Z \to \infty$. We do not require the numerical value of $B$; to find it, a more detailed calculation would be required.

### B. The matched solution

To see in more detail how the finger solution is matched to the thread solution, we use the standard procedure (Ref. 25, p. 57) of introducing an intermediate variable

$$\overline{\xi} = \frac{z' - z'_m}{\Delta^{(ax)}_{match}} \equiv \frac{z' - z'_m}{t'^{3/4}},$$

and expanding both the inner and outer solutions in $\overline{\xi}$. As can be seen in Fig. 1, the end of the thread solution at $z'_m$ is shifted relative to the tip at $z'_{tip}$, owing to the presence of the rounded finger solution. The shift between the two, which is $Z_m$ in the inner variable, will be determined from volume conservation below, and we have

$$z'_m - z'_{tip} = t\,Z_m. \tag{52}$$

Then at constant $\overline{\xi}$, the outer variable $\Delta\xi = \overline{\xi}t'^{3/4-\beta}$ goes to zero, while the inner variable $Z = \overline{\xi}t'^{-1/4} + Z_m$ tends to infinity. Now expansion of the outer solution yields according to (25)

$$h = t'r_0\phi_a(\Delta\xi) = t'r_0\left[\frac{1}{6} + \chi_m\left(\frac{\overline{\xi}}{36}\right)^{1/(2+\beta)} t'^{\frac{3-4\beta}{8+4\beta}} + \dots\right] \approx \frac{t'r_0}{6} \tag{53}$$

for $t' \to 0$. On the other hand, according to (51) the inner solution behaves as

$$h = t'r_0R(Z) = t'r_0R(\overline{\xi}t'^{-1/4} + Z_m) = t'r_0\left[\frac{1}{6} + \frac{Bt'^{1/4}}{\overline{\xi}} + \dots\right] \approx \frac{t'r_0}{6}, \tag{54}$$

which is identical to (53) in the limit $t' \to 0$. Note that the corrections to the leading behavior $t'r_0/6$ do not match between (53) and (54), as the equations they are based upon are themselves valid to leading order in $t'$ only.

Having established that both inner and outer solutions have the same functional form in the overlap region, it remains to determine the relative horizontal position of one solution relative to the other, which is set by $Z_m$, cf. (52). Observe that the thread solution (15) conserves volume exactly, as the tip is located at $s' = 0$, which is a constant. Thus if $s' = s_+$ is another particle label away from the point of breakup, where the solution is essentially static, the total volume is

$$V = \int_{z_m}^{z_+} h^2 dz = \int_0^{s_+} ds = s_+,$$

which is constant. Using volume conservation, we can determine the placement of the finger solution: for any $t'$, the volume of the full solution must be that of the thread solution (15). This procedure is illustrated on the left of Fig. 3, where the dashed line shows a cylinder of radius 1/6, which has the same volume as the finger solution. This means that the apex of the finger solution is shifted relative to a cylinder of constant radius by a distance $Z_m$ in similarity variables. Rewriting (52) slightly, we find that the true tip position is at

$$z'_{tip} = \xi_m t'^{\beta} - t' Z_m. \tag{55}$$

We now show that $Z_m = V_m/3$, with the velocity shift $V_m \approx 0.25$ found above. Namely, the similarity form of the velocity profile away from the tip is $-2Z + V_m$, which must coincide with the velocity profile inside the cylinder solution (dashed line on the left of Fig. 3); this linear profile conserves volume exactly for a constant radius $R = 1/6$. Thus the velocity at $Z_m$, at the end of the cylinder, is $-2Z_m + V_m$. However, since the end of the cylinder moves like $tZ_m$, we have $-2Z_m + V_m = Z_m$, as claimed. By differentiating (55), we find the velocity of the tip, which is smaller by a correction $-Z_m$ relative to the leading order estimate (20).

Note that it is consistent to compare the volume of the finger solution to that of a cylinder of constant radius, which corresponds to the leading-order term in (25). Taking into account the first correction, the volume up to a scale $t'$ from the tip (which is the scale of the finger solution) is

$$\int_{z'_m}^{z'_m+t'} h^2 dz \approx \frac{t'^3}{36} r_0^3 \left[1 + \frac{36^{1-1/\delta}\chi_m}{3(1+1/\delta)} t'^{3/\delta-1}\right].$$

But $3/\delta - 1 \approx 0.38$, and so the correction goes to zero with $t' \to 0$.

### C. Composite solution

Now we are in a position to construct a solution to the receding thread problem which is valid uniformly in space, combing the inner and outer solutions.[25] The idea is to add the two solutions together, and to subtract the function valid in the overlap region, which is $h = t' r_0/6$. Taking into account the shift (55) of the tip position relative to $\xi_m t'^{\beta}$, this leads to the global or composite solution

$$\frac{h_{comp}}{r_0} = t' R\left(\frac{z' - z'_{tip}}{t'}\right) + t' \begin{cases} 0, & z' - z'_{tip} \le Z_m t' \\ \phi_a\left(\frac{z'-z'_{tip}}{t'^{\beta}} - t'^{1-\beta} Z_m\right) - \frac{1}{6}, & z' - z'_{tip} > Z_m t' \end{cases}, \tag{56}$$

shown as the solid line in Fig. 1. It is seen that (56) matches smoothly between the finger solution (dotted line) as the apex is approached, while merging with the thread solution (21) on scales greater than the tip size $t' r_0/6 \approx 0.017$. Note the disparity in scale between the size of the inner solution and the axial extend of the thread.

To construct the globally valid solution for the $z$-component $v_z$ of the velocity field, we have to add the outer solution (29) to the inner solution (41), subtracting the velocity in the overlap region. To find the latter, note that taking the time derivative of (55) the velocity at the tip is $v_{tip}/v_\eta = v_m/v_\eta - Z_m$. According to the above, the limit of the inner velocity away from the tip is $V_m - 2Z = 3Z_m - 2Z$. Combining the two, we obtain the $z$-velocity in the overlap region as

$$v/v_\eta = v_m/v_\eta + 2(Z_m - Z), \quad Z = \frac{z' - z'_{tip}}{t'}. \tag{57}$$

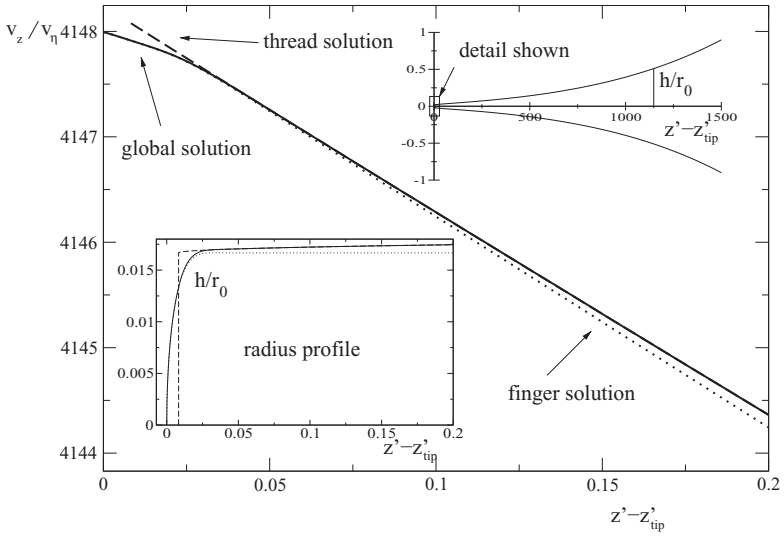


FIG. 4. The $z$-component $v_z$ of the velocity on the surface of the receding thread for $t' = 0.1$. as described by (21) and (23). The inset shows how the finger solution is fitted in, on a much smaller scale set by $t'$. The thread solution (21), shown as the dashed line, is almost perfectly cylindrical on this scale. The finger solution (40) is fitted in such that volume is conserved.

The overlap velocity (57) is also obtained from the outer solution (41), by taking the limit of small $\Delta\xi$ in the expansion (33). Thus, we obtain the following composite solution for the velocity,

$$\frac{v_{comp}}{v_\eta} = \frac{v_{tip}}{v_\eta} + V_z(Z) + \begin{cases} 0, & Z \le Z_m \\ t'^{\beta-1}\left[\psi_a\left(\frac{z'-z'_{tip}}{t'^\beta} - t'^{1-\beta}Z_m\right) - \psi_m\right] + 2(Z_m - Z), & Z > Z_m \end{cases}, \tag{58}$$

shown in Fig. 4 for $t' = 0.1$. Once more the global solution is seen to interpolate smoothly between inner and outer solutions. Once more, note the extremely high speed of retraction, although the value of $t'$ is quite modest.

This completes our description of the case where inertia is negligible. However, even if the viscosity is very large, inertia will become relevant sufficiently close to the singularity.[2] The reason is that according to the Stokes solution, the inertial term in the Navier-Stokes equation grows faster than the viscous term, so the approximation is no longer self-consistent once they have become of the same order. Thus on a sufficiently small scale, or for fluids whose viscosity is not very large, inertia has to be included in the description.

## IV. NAVIER-STOKES CASE

### A. Thread solution

In the case that inertia is included, the outer (thread) solution has to be replaced by another similarity solution:[19]

$$h(z,t) = \ell_\nu t' \phi_a\left(\frac{z'}{t'^{1/2}}\right), \quad v(z,t) = \frac{\ell_\nu}{t_\nu} t'^{-1/2} \psi_a\left(\frac{z'}{t'^{1/2}}\right), \tag{59}$$

with the intrinsic length and time scales $\ell_\nu$ and $t_\nu$, respectively. We will in this section refer to (59) as the thread solution, and once more denote the similarity profile of the post-breakup Navier-Stokes solution by $\phi_a$. The dimensionless time distance is now $t' = (t - t_0)/t_\nu$, and $z' = (z - z_0)/\ell_\nu$. Since the radial scale $t'$ is much smaller than the axial scale $t'^{1/2}$ for small $t'$, long-wavelength equations[14] can be applied. We will see that as far as the tip region of the thread solution is concerned, all results of Secs. II and III carry over, but with the exponent $\beta \approx 0.175$ being replaced by $\beta = 1/2$. The reason is that near the tip, the Navier-Stokes solution is dominated by viscosity, so the equations are

effectively the same, except that the axial length scale is somewhat shorter, but still asymptotically large compared to the radial scale. Inserting (59) into the long-wavelength equations, one obtains a pair of ordinary differential equations for $\phi_a$, $\psi_a$:[19]

$$\phi_a - \xi\phi_a'/2 + \psi_a\phi_a' = -\psi_a'\phi_a/2, \tag{60}$$

$$-\frac{\psi_a}{2} - \frac{\xi\psi_a'}{2} + \psi_a\psi_a' = \phi_a'/\phi_a^2 + 3\frac{(\psi_a'\phi_a^2)'}{\phi_a^2}, \tag{61}$$

which determine the shape of the receding thread. However, appropriate boundary conditions still need to be found at the tip.

As in the Stokes case, the radial variable is proportional to $t'$, and the radius at the end of the thread solution is

$$h_m = \ell_v t'\phi_a(\xi_m) = v_\eta(t - t_0)\phi_a(\xi_m). \tag{62}$$

Since for $t' \to 0$ the axial scale is again much larger than the radial scale, the tip region of the thread solution looks like a cylinder of constant radius $\phi_a(\xi_m)$. Requiring it to match to the finger solution (40), which has the asymptotic radius $h_f = v_\eta t/6$, it follows that

$$\phi_a(\xi_m) = 1/6, \tag{63}$$

as was concluded in Ref. 19.

### B. Matching

We now show that on the matching scale $\Delta_{match}^{(ax)} = t'^{3/4}$, intermediate between the axial scale of the finger solution $t'$ and that of the thread solution $t'^{1/2}$, inertia drops out and we are allowed to use the same finger solution (40) as in the Stokes case. This is to be expected on the basis of the scaling given in Ref. 15, where the Stokes length over which a finger of constant radius persists (as opposed to a "blob") is given by $\sqrt{\ell_v h} \approx \sqrt{\ell_v t'/6} \gg \Delta_{match}^{(ax)}$.

To show this explicitly and to make sure that the two descriptions match on the scale $\Delta_{match}^{(ax)}$, we demonstrate that a solution of (60), (61) agrees with the finger solution for large $Z$. To perform this comparison, we have to pass into a frame of reference moving with the tip. Since the end is at $z_m' = \xi_m t'^{1/2}$, it moves at speed $v_m/v_\eta = \xi_m t'^{-1/2}/2$. In similarity variables, the scale $\Delta_{match}^{(ax)}$ corresponds to $t'^{1/4}$; therefore, if we introduce the intermediate variable $\bar{\xi} = t'^{-1/4}(\xi - \xi_m)$, the distance $\Delta_{match}^{(ax)}$ from the tip is a time-independent quantity. The transformation of the profiles to the variable $\bar{\xi}$ reads

$$\bar{\phi}(\bar{\xi}) = \phi_a(\bar{\xi} + \xi_m), \quad \bar{\psi}(\bar{\xi}) = t'^{-1/4}\left(\psi_a(\bar{\xi} + \xi_m) - \xi_m/2\right), \tag{64}$$

and in rescaled variables, the similarity equations (60), (61) become

$$\overline{\phi} - \overline{\xi\phi}'/2 + \overline{\psi\phi}' = -\overline{\psi}'\overline{\phi}/2 \tag{65}$$

$$t'^{1/2}\overline{\phi}^2\left[-\overline{\psi}/2 - \overline{\xi\psi}'/2 + \overline{\psi\psi}'\right] - t'^{1/4}\overline{\phi}^2\xi_m/4 = \left\{\overline{\phi} + 3\overline{\psi}'\overline{\phi}^{-2}\right\}', \tag{66}$$

respectively.

The tip region (of size $t'$) corresponds to the limit $\bar{\xi} \to 0$. Since by construction, $\overline{\psi}(0) = 0$, expanding to linear order we find $\overline{\psi} \propto \bar{\xi}$. Thus, to leading order as $\bar{\xi} \to 0$, (65) yields $\overline{\phi} = -\overline{\psi}'\overline{\phi}/2$, so it follows that

$$\overline{\psi} = -2\bar{\xi} + \text{higher order terms}. \tag{67}$$

In terms of $\psi_a$, this means that

$$\psi_a = \xi_m/2 - 2(\xi - \xi_m) + \text{higher order terms}. \tag{68}$$

On the other hand, in the limit $t' \to 0$ inertial terms drop out, and (66) becomes

$$\overline{\phi} + 3\overline{\psi}'\overline{\phi}^2 = \overline{T}, \tag{69}$$

where $\overline{T}$ is a constant of integration. Comparison to (11) shows that $\overline{T}$ corresponds to the tensile force in the thread. Since the free end cannot support a force, its value must be zero. Indeed, inserting $\overline{\phi} = 1/6$ on account of (63), as well as (67), shows that $\overline{T} = 0$, in agreement with (11). Converting (67) to real space, we find on the scale of the tip:

$$\frac{v - v_m}{v_\eta} = t'^{-1/2}(\psi_a - \xi_m/2) = t'^{-1/4}\overline{\psi} = -2t'^{-1/4}\overline{\xi} = -2t'^{-1/2}(\xi - \xi_m) = -2\frac{z' - z'_m}{t'},$$

which matches the far field behavior (57) of the finger solution.

In conclusion, we have to solve (60), (61) subject to the conditions (63), (68) at the tip, which are the conditions derived in Ref. 19, but using a more *ad hoc* argument. We will recapitulate only very briefly the main results of Ref. 19. An expansion around $\xi_m$ gives

$$\phi_a = 1/6 + \phi_1(\xi - \xi_m)^{2/5} + O(\xi - \xi_m)^{3/5}, \tag{70}$$

note that the exponent 2/5 agrees with the exponent $1/\delta = 1/(2+\beta)$ in (25), if we put $\beta = 1/2$, as is appropriate for the Navier-Stokes solution. This is to be expected, since the two similarity solutions are in fact equivalent near the tip, as we have demonstrated.

Together with (68), (70) determines the thread solution in terms of two free parameters $\xi_m$ and $\phi_1$. These two parameters are determined uniquely by the requirement that the post-breakup solution has to match the pre-breakup solution $\phi_b$,$\psi_b$ for $\xi \to \pm\infty$. Since the solution is asymmetric in the Navier-Stokes case, this leads to two different solutions on the left and right of the point of breakup (or vice versa).

Namely, the behavior of the pre-breakup solution is

$$\left.\begin{aligned} \phi(\xi)/\xi^2 &\to a_0^{\pm} \\ \psi(\xi)\xi &\to b_0^{\pm} \end{aligned}\right\} \quad \text{for} \quad \xi \to \pm\infty. \tag{71}$$

On one side the solution is very flat (which by convention we are taking as the limit $\xi \to -\infty$), corresponding to a fluid thread, while on the other side $a_0$ is much larger, where the solution matches to a drop, see Fig. 5 below. The pre-breakup solution selects unique values of the constants $a_0^{\pm}$ and $b_0^{\pm}$, for example, $a_0^- \approx 6.047 \times 10^{-4}$ for the thread side, and $a_0^+ \approx 4.635$ for the drop side.[19] Adjusting $\xi_m$ and $\phi_1$ on either side such that integration of (60), (61) yields the same constants

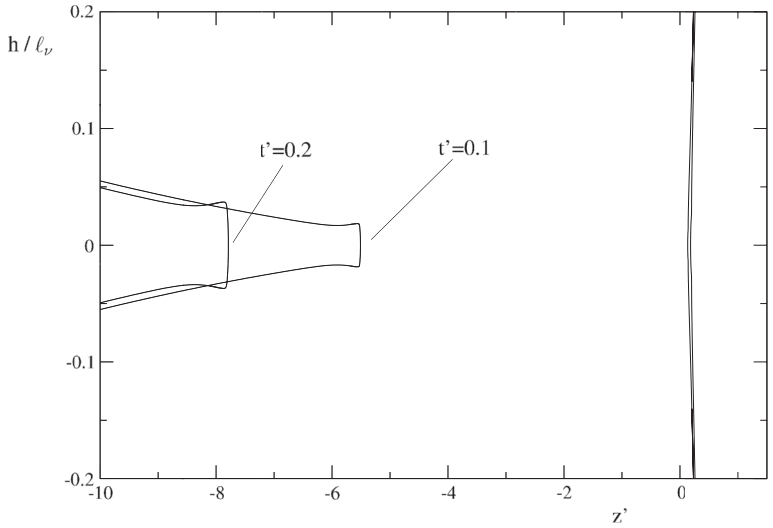


FIG. 5. The composite post-breakup solution for the Navier-Stokes case. Note the strong asymmetry; on the left is the "thread," on the right the "drop.'.

$a_0^{\pm}, b_0^{\pm}$, we find[19] $\xi_m^- \approx 17.452$, $\phi_1^- \approx 0.06183$ for the thread, and $\xi_m^+ \approx 0.4476$, $\phi_1^+ \approx 0.6180$ for the drop side. This completes the construction of the post-breakup solution in the Navier-Stokes case.

### C. Composite solution

To construct a global solution, valid uniformly, we proceed similar to the Stokes case, as in Subsection III C. Namely, we add the two solutions together, and subtract the solution in the overlap region, which in our case is the constant solution $h = \ell_\nu t'/6$. The outer solution is the thread solution (59), which has an axial scaling exponent $\beta = 1/2$. As described above, two very different similarity profiles $\phi_a(\xi)$ are produced by using boundary conditions at the tip appropriate for the thread and the drop side of the problem.

The inner solution is the finger solution (40), which can be written in the form

$$h(z', t') = \ell_\nu t' R\left(\frac{z' - z'_{tip}}{t'}\right), \tag{72}$$

where $R(Z)$ is the finger profile shown in Fig. 3. Note that in the Navier-Stokes solution, time is non-dimensionalized using $\ell_\nu$, so that $t' = (t - t_0)/t_\nu$.

Then the result for the global or composite solution is

$$h_{comp} = \ell_\nu t' R\left(\frac{z' - z'_{tip}}{t'}\right) + \ell_\nu t' \begin{cases} 0, & z' - z'_{tip} \le Z_m t' \\ \phi_a\left(\frac{z'-z'_{tip}}{t'^{1/2}} - t'^{1/2} Z_m\right) - \frac{1}{6}, & z' - z'_{tip} > Z_m t' \end{cases}, \tag{73}$$

which is plotted in Fig. 5; note the tip which is rounded slightly. The tip position $z_{tip}$ is given by (55), but with $\beta = 1/2$:

$$z'_{tip} = \xi_m t'^{1/2} - t' Z_m. \tag{74}$$

## V. DISCUSSION

We begin by discussing the different types of solutions expected to be observed as function of the Ohnesorge number (1), which is a non-dimensional measure of the size of the viscosity. The relative size of the viscous, inertial, and surface tension contributions after breakup mirrors the transitions observed as breakup is approached,[2] but in reverse order. Namely, the size of inertial and viscous contributions in the long-wavelength equation is given by $\rho v v_z$ and $\eta v_{zz}$, respectively. Evaluating both terms for the Stokes solution, one finds that inertia dominates, if[2]

$$\frac{t - t_0}{\ell_\nu} \lesssim Oh^{\frac{4-4\beta}{2\beta-1}}. \tag{75}$$

This quantifies our earlier statement that even at large viscosities, the Navier-Stokes solution is observed first. Only after the time estimated by (75) does a crossover to the Stokes solution occur.

A similar argument applies to the case of very small $Oh$. If one estimates the relative size of viscous and inertial terms based on the inviscid similarity solution,[11] one finds that viscosity becomes important if

$$\frac{t - t_0}{\ell_\nu} \lesssim 1. \tag{76}$$

Thus, the Navier Stokes solution once more applies at very early times, but crosses over to the inviscid solution once the tip size becomes comparable to the viscous length $\ell_\nu$, which is about 10 nm for water. If the Ohnesorge number is of order one, one still has the requirement that the thread width must be much smaller than the external scale $r_0$, for the similarity approach to apply.

The asymmetry of the two sides of the post-breakup solution in the Navier-Stokes case is illustrated in Fig. 5. The "thread" side is very flat, while the profile on the "drop" side grows very quickly. However, note the difference in scale of the radial and axial axes of Fig. 5. In fact, the profile

on the right is still slender. The asymmetry of the breakup has important practical consequences, for example, for the breakup of liquid jets. In the surface tension driven breakup of jets one observes a sequence of drops, separated by slender necks; at elevated viscosities the necks become thinner and thread-like.[2] This pattern matches neatly with the asymmetric post-break solution shown in Fig. 5: it is clear that the left part of the solution matches well onto the neck, the right onto the drop.

The thread solution dictates that the point of breakup is close to the drop, from where the neck will be receding. Almost at the same time, a corresponding event will occur at the next drop, but with a thread solution that is flipped over. Eventually, almost the entire neck recedes into another, smaller drop, which is known as the "satellite" drop. Hence the outcome of jet breakup is typically a sequence of "main" drops, separated by smaller satellite drops.[2] This bimodal distribution of drops adversely affects the quality of ink-jet printing, since different drop sizes are guided to different locations, producing a diffuse image.

Experimental verification of the thread retraction has proved difficult.[2] The reasons are twofold: first, in the case of high viscosities an instability sets in during pinching of the thread, driven by thermal noise or other random perturbations.[7] As a result, the thread is often observed to break at several places, making it difficult to clearly identify a similarity solution. Second, the retraction speed of the thread predicted by (74) is quite high, placing high demands on the temporal resolution. For a typical experiment analyzed in Ref. 31, 6.7 $\mu$s after breakup, the speed is about 37 m/s. As a result, the effect of air drag on the thread might be important. High retraction speeds are due to the fact that $\xi_m^- \approx 17.5$ is quite large; it would be worthwhile to track the tip of the other (drop) side carefully, whose speed at the same value of $t'$ is smaller by about a factor of 1/40. Note that the speeds in the Stokes case are even larger, as the prefactor $A$ in (20) is about 621, and the exponent $\beta - 1 \approx -0.825$ is more negative.

A possible resolution is to work with fluids at moderate values of the viscosity, so that inviscid breakup is observed at first, which then crosses over to the Navier-Stokes breakup we are interested in. For example, experiments were reported in Ref. 6 at an Ohnesorge number $Oh \approx 0.163$, and no effect of random breakup was observed. In agreement with (76), the transition to the Navier-Stokes regime occurs when the minimum thread radius is about $\ell_\nu \approx 96$ $\mu$m. The thermal instability is expected to set in a threshold radius of about

$$h_{thres} = 5\ell_\nu \left(\frac{\ell_T}{\ell_\nu}\right)^{0.4},$$

where $\ell_T = \sqrt{k_B T/\gamma}$ is a thermal length which is about a nanometer at room temperature. As a result, instability is predicted to set in at about $h_{thres} \approx 0.05\ell_\nu$, which would leave a considerable range for the thread solution to develop.

## ACKNOWLEDGMENTS

I am very grateful to Howard Stone, who first suggested the similarity solution describing the recoil of a cylindrical drop, shown in Fig. 2.

[1] O. A. Basaran, "Small-scale free surface flows with breakup: Drop formation and emerging applications," AIChE J. **48**, 1842 (2002).
[2] J. Eggers and E. Villermaux, "Physics of liquid jets," Rep. Prog. Phys. **71**, 036601 (2008).
[3] J. Eggers, "Universal pinching of 3D axisymmetric free-surface flow," Phys. Rev. Lett. **71**, 3458 (1993).
[4] T. A. Kowalewski, "On the separation of droplets," Fluid Dyn. Res. **17**, 121–145 (1996).
[5] A. Rothert, R. Richter, and I. Rehberg, "Formation of a drop: Viscosity dependance of three flow regimes," New J. Phys. **5**, 59 (2003).
[6] A. U. Chen, P. K. Notz, and O. A. Basaran, "Computational and experimental analysis of pinch-off and scaling," Phys. Rev. Lett. **88**, 174501 (2002).
[7] M. P. Brenner, X. D. Shi, and S. R. Nagel, "Iterated instabilities during droplet fission," Phys. Rev. Lett. **73**, 3391 (1994).
[8] J. R. Lister and H. A. Stone, "Capillary breakup of a viscous thread surrounded by another viscous fluid," Phys. Fluids **10**, 2758 (1998).
[9] Y.-J. Chen and P. H. Steen, "Dynamics of inviscid capillary breakup: Collapse and pinchoff of a film bridge," J. Fluid Mech. **341**, 245–267 (1997).
[10] R. F. Day, E. J. Hinch, and J. R. Lister, "Self-similar capillary pinchoff of an inviscid fluid," Phys. Rev. Lett. **80**, 704 (1998).

[11] A. Sierou and J. R. Lister, "Self-similar recoil of inviscid drops," Phys. Fluids **16**, 1379 (2004).
[12] J. B. Keller and M. J. Miksis, "Surface tension driven flows," SIAM J. Appl. Math. **43**(2), 268–277 (1983).
[13] J. Billingham, "Surface tension-driven flow in a slender wedge," SIAM J. Appl. Math. **66**, 1949–1977 (2006).
[14] J. Eggers and T. F. Dupont, "Drop formation in a one-dimensional approximation of the Navier-Stokes equation," J. Fluid Mech. **262**, 205 (1994).
[15] M. P. Brenner and D. Gueyffier, "On the bursting of liquid films," Phys. Fluids **11**, 737–739 (1999).
[16] R. Stocker and A. E. Hosoi, "Lubrication in a corner," J. Fluid Mech. **544**, 353 (2005).
[17] J. D. Paulsen, R. Carmigniani, A. Kannan, J. C. Burton, and S. R. Nagel, "Coalescence of bubbles and drops in an outer fluid," Nat. Commun. **5**, 3182 (2014).
[18] N. Marheineke and R. Wegener, "Asymptotic model for the dynamics of curved viscous fibres with surface tension," J. Fluid Mech. **622**, 345–369 (2009).
[19] J. Eggers, "Theory of drop formation," Phys. Fluids **7**, 941 (1995).
[20] D. T. Papageorgiou, "Analytical description of the breakup of liquid jets," J. Fluid Mech. **301**, 109 (1995).
[21] G. I. Taylor, "The dynamics of thin sheets of fluid III. Disintegration of fluid sheets," Proc. R. Soc. London **253**, 313–321 (1959).
[22] J. B. Keller, "Breaking of liquid films and threads," Phys. Fluids **26**, 3451–3453 (1983).
[23] L. Ting and J. B. Keller, "Slender jets and thin sheets with surface tension," SIAM J. Appl. Math. **50**, 1533 (1990).
[24] J. B. Keller, A. King, and L. Ting, "Blob formation," Phys. Fluids **7**(1), 226 (1995).
[25] E. J. Hinch, *Perturbation Methods* (Cambridge University Press, Cambridge, 1991).
[26] D. T. Papageorgiou, "On the breakup of viscous liquid threads," Phys. Fluids **7**, 1529 (1995).
[27] J. Eggers, "Stability of a viscous pinching thread," Phys. Fluids **24**, 072103 (2012).
[28] C. Clasen, J. Eggers, M. A. Fontelos, J. Li, and G. H. McKinley, "The beads-on-string structure of viscoelastic jets," J. Fluid Mech. **556**, 283 (2006).
[29] J. Eggers and M. A. Fontelos, "Isolated inertialess drops cannot break up," J. Fluid Mech. **530**, 177 (2005).
[30] C. E. Weatherburn, *Differential Geometry of Three Dimensions* (Cambridge University Press, Cambridge, 1939), Vol. I.
[31] J. Eggers, "Nonlinear dynamics and breakup of free-surface flows," Rev. Mod. Phys. **69**, 865–929 (1997).
[32] A. Erdelyi, *Higher Transcendental Functions* (McGraw-Hill, New York, 1953).
[33] I. S. Gradshteyn and I. M. Ryzhik, *Table of Integrals Series and Products* (Academic, New York, 1980).
[34] R. M. S. M. Schulkes, "The contraction of liquid filaments," J. Fluid Mech. **309**, 277 (1996).
[35] P. Notz and O. A. Basaran, "Dynamics and breakup of a contracting liquid filament," J. Fluid Mech. **512**, 223 (2004).